Original Research Article: full paper

(2023), «EUREKA: Physics and Engineering»
Number 3

DEVELOPMENT OF MECHANICAL PROPERTY PREDICTION MODEL AND OPTIMIZATION FOR DISSIMILAR ALUMINUM ALLOY JOINTS WITH THE FRICTION STIR WELDING (FSW) PROCESS

Yodprem Pookamnerd
Faculty of Industrial Technology[1]

Panuwat Thosa
Faculty of Industrial Technology[1]

Sittichai Charonerat
Faculty of Industrial Technology[1]

Suriya Prasomthong✉
Faculty of Industrial Technology[1]
Suriya.p@npu.ac.th

[1]*Nakhon Phanom University*
214 Chayangkun str., Mueang District, Nakhon Phanom, Thailand, 48000

✉**Corresponding author**

Abstract

Friction stir welding (FSW) is a solid-state joining process used to weld dissimilar aluminum alloys with varying material properties and compositions. Unlike traditional welding methods, FSW does not involve melting the materials being welded but instead uses a rotating tool to heat and stir the materials until they are in a plastic state. The process results in a welded joint with high strength, excellent ductility, and minimal distortion, making it a popular choice in various industries, including aerospace, automotive, and marine. AA6061-T6 (Mg-Si) and AA7075 (Al-Zn-Mg-Cu) aluminum alloys are one of the most popular grades of aluminum alloys used in current manufacturing industries, such as aerospace and automotive, joined by the Friction Stir Welding Process (FSW) technique. Taguchi orthogonal array (L9) experimental design was applied to reduce the number of insignificant factors in the process. First, the study determines three welding factors: rotation speed, travel speed, and pin eccentricity. Investigations found that travel speeds significantly on tensile strength (*Ts*) and elongation (% El), but the rotational speed and tool eccentricity did not affect Ts and % El. Furthermore, considering the fabricated parameters on the hardness (HV) of the joint, it was found that all factors unaffected the HV of the joint zone at a 95 % confidence level. Next, examine the microstructure; Mg_2Al_3 and Al_2O_3 intermetallic compounds were found in the weld. Therefore, investigating the crystallite size found that welding significantly affects the crystallite size. Finally, consider the fracture surface, experimental condition $A_2B_1C_2$ (optimal parameter), which is the parameter with the highest tensile strength having dimple fracture characteristics. On the other hand, the welding condition $A_1B_3C_3$, the parameter with the lowest tensile strength, Small and fine dimple fracture with cleavage fracture. Because the material is highly ductile and can undergo large deformations before it is damaged. On the other hand, materials with low tensile strength exhibiting cleavage fracture indicate that the materials are brittle and can break easily under stress.

Keywords: optimization, dissimilar joint, aluminum alloy, friction stir welding, mechanical property, prediction model.

DOI: 10.21303/2461-4262.2023.002776

1. Introduction

Currently automotive, aerospace, shipbuilding, and other industries are focusing on reducing the weight of parts to reduce fuel consumption. In addition, converting energy from fuel to electricity is, therefore, necessary to reduce the weight of the parts. This has led to lightweight materials such as aluminum and aluminum alloys, the most popular lightweight materials widely used in industry. Due to many unique properties such as lightweight, corrosion resistance, and high strength to weight [1, 2]. The most commonly used aluminum alloys in the industry are AA6061-T6 (Mg-Si) [1, 3] and AA7075 (Al-Zn-Mg-Cu) aluminum alloys. This is the strength of aluminum alloy used in manufacturing at present. In addition, AA7075 aluminum alloy has

a high strength to weight and resistance to natural aging, making it attractive for use in the aerospace industry [4, 5].

Dissimilar aluminum joints begin with riveting, adhesion, and resistance spot welding (RSW) [6, 7]. However, the Friction stir welding (FSW) technique has recently been proven to be one of the best methods for joining dissimilar aluminum [8, 9]. Because, as a solid-state welding technique, it eliminates welding defects such as solidification cracking, thermal distortion, porosity, hot crack, and brittle intermetallic compound (IMC) [10]. In addition, the welds that were established have a good surface finish, so post-weld cleaning is not required. Welding principles with FSW process welding tools have three components: shaft, shoulder, and pin. The shaft clamps the shoulder, and the pin generates heat from friction on the workpiece. The tool shoulder is primarily responsible for generating heat and causing plastic deformation in the weld zone. Simultaneously, the pin acts as a stirrer to mix the materials until a joint is formed [11]. When the welding direction and tool rotation are similar, it is known as the advancing side (AS). On the other hand, dissimilar welding and rotation directions are known as restirring sides (AS). In addition, joints fabricated from the FSW process have increased ductility. However, the tensile strength is slightly lower than the base metals. The fine microstructure is obtained from dynamic crystallization during stirring [12]. The overall welding factors are tool profile, rotation speed, travel speed, holding time, tilt angle, and plunge depth, which often on the microstructure and mechanical properties of the joint [13–16].

A large number of studies have been conducted for optimizing joint fabrication by techniques such as the fabrication factor using Taguchi [17–19], response surface methodology (RSM) [20–22], Full factorial design techniques [23–25], Artificial Neural Networks (ANN) [26, 27], or adaptive neuro-fuzzy inference system (ANFIS) [28, 29]. These processes have been demonstrated to be able to model appropriately to predict the response of the FSW process. Compared to predictive modeling techniques, the Taguchi method is interesting because it is simple, reduces the number of trials, and reduces the variability of the trials. By selecting the control factor, the data will be converted into the Signal to Noise (*S*/*N* Ratio) search for finding the correct factor to find the optimal value. Currently, the Taguchi technique is still used for determining the optimum factors in the FSW process; for example, examined joints of aluminum alloy AA5083 and AA7075 using the FSW process [30]. The Taguchi technique was used to determine the welding parameters: rotational speed, feed, and tool tilt angle. Taguchi's method confirmed that rotational speed was the most critical parameter than the tools feed and tilt angle [30]. Used the Taguchi technique to predict AA6061 and AA7075 aluminum alloy joints with the FSW process [31]. Studied the tensile strength of the FSW process joint of aluminum alloy AA6061 by the Taguchi technique [32]. For joining titanium and aluminum alloys with FSSW welding using Taguchi technique experimental design. It was found that the Taguchi method could predict experimental results effectively [33]. The Taguchi method also used to create a mathematical model to predict the tensile strength and hardness of the AA5083 semi-solid cast aluminum welded joint using the FSW process [34]. However, many other studies have chosen the Taguchi method for modeling and predicting responses [35–37].

Therefore, this study uses the methods and concepts above to study the FSW process using aluminum alloys AA6061-T6 and AA7075 in the experiment. Welding parameters are welding speed, travel speeds, and pin eccentricity. Because these parameters determine the strength of the joint. Analyze the *S*/*N* ratio by the Taguchi method and analysis of variance (ANOVA). Because ANOVA (Analysis of Variance) is a statistical method used to determine the significant difference between the mean of a sample. Regression equations were constructed to predict tensile strength, elongation, and weld hardness to determine the optimum parameters of the weld toward joint quality. Finally, the appropriate parameters were used in repeated experiments to confirm the results. The chemical composition and crystallite size were investigated by XRD and the joint fracture characteristics by SEM/EDX.

2. Materials and methods

2. 1. Experimental materials

AA6061-T6 and AA7075 aluminum alloys were the base materials used for this study. The microstructures are shown in **Fig. 1,** and the chemical composition are shown in **Table 1**.

The size of the experimental specimens was 75×150×6 mm. It was cut by a band saw and milled by a CNC machine using coolant. The mechanical properties of the experimental materials are shown in **Table 2**; pre-welding, the specimens are cleaned with acetone.

Table 1
Chemical compositions of AA6061-T6 and AA7075 Aluminum alloys

Material	% Element (% wt)								
	Cr	Cu	Fe	Mg	Mn	Si	Ti	Zn	Al
AA6061-T6	0.17	0.28	0.33	0.90	0.06	0.62	0.02	0.02	Bal.
AA7075	0.063	0.17	0.24	0.86	0.12	0.54	N/A	0.12	Bal.

Table 2
Mechanical properties of AA6061-T6 and AA7075 Aluminum alloys

Material	Mechanical properties			
	Ultimate tensile strength (MPa)	Yield strength (MPa)	% Elongation	Hardness (HV)
AA6061-T6	334	302	12.24	105
AA7075	512	467	8.24	178

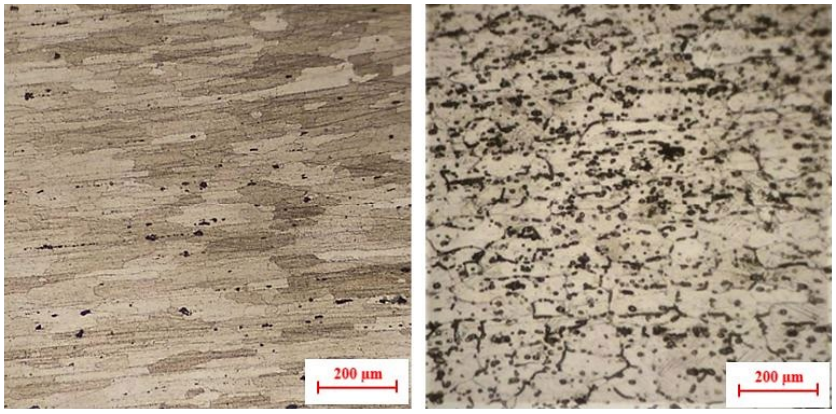

a *b*

Fig. 1. The microstructures of the base material: *a* – AA7075; *b* – AA6061-T6

2. 2. Welding and testing process

The dimensions and characteristics of the joint are shown in **Fig. 2**. (Design an experimental process with Solid Work software.) Next, clamp the welding specimens on the clamping equipment on the CNC milling machine Table (Model: VMC MACHINE CYCLONE-610). Next, adjust the clamping equipment on the workTable with a dial gauge and clamp with a screw. Therefore AA6061-T6 and AA7075 aluminum alloy specimens are fixed on the fixture, as shown in **Fig. 2, *a***, Program the operation of the machine and adjust the parameters according to the specified variables. The constant welding parameter was determined according to the literature review [20]; the holding time was 10 sec. The welding tool shape is a threaded cylinder fabricated from SKD-11 tool steel, as shown in **Fig. 2, *b.*** Next, determine the direction of the left-hand tool rotation and shoulder plunge depth to a surface of 0.3 mm.

The parameters in this study, shown in **Table 3**, include tool rotational speed, travel speeds, and pin eccentricity. These parameters are based on relevant research [20, 34].

Therefore, the specimens were prepared for mechanical and chemical properties testing. The segmentation cutting distance is shown in **Fig. 2, *c***. Tensile strength test according to ASTM E 8M standard, three pieces to determine the average on a universal testing machine, model: HD B616-2-60T, at Nakon Phanom University, Thailand. The strain rate in the tensile test was 15 s^{-1}, and Micro Vickers was used to examining joint hardness. Investigate at BM, HAZ,

TMAZ and SZ both Advancing and Retreating side, test distance 0.2 mm, using 0.98 kgf, for 10 sec according to ASTM E384 standard.

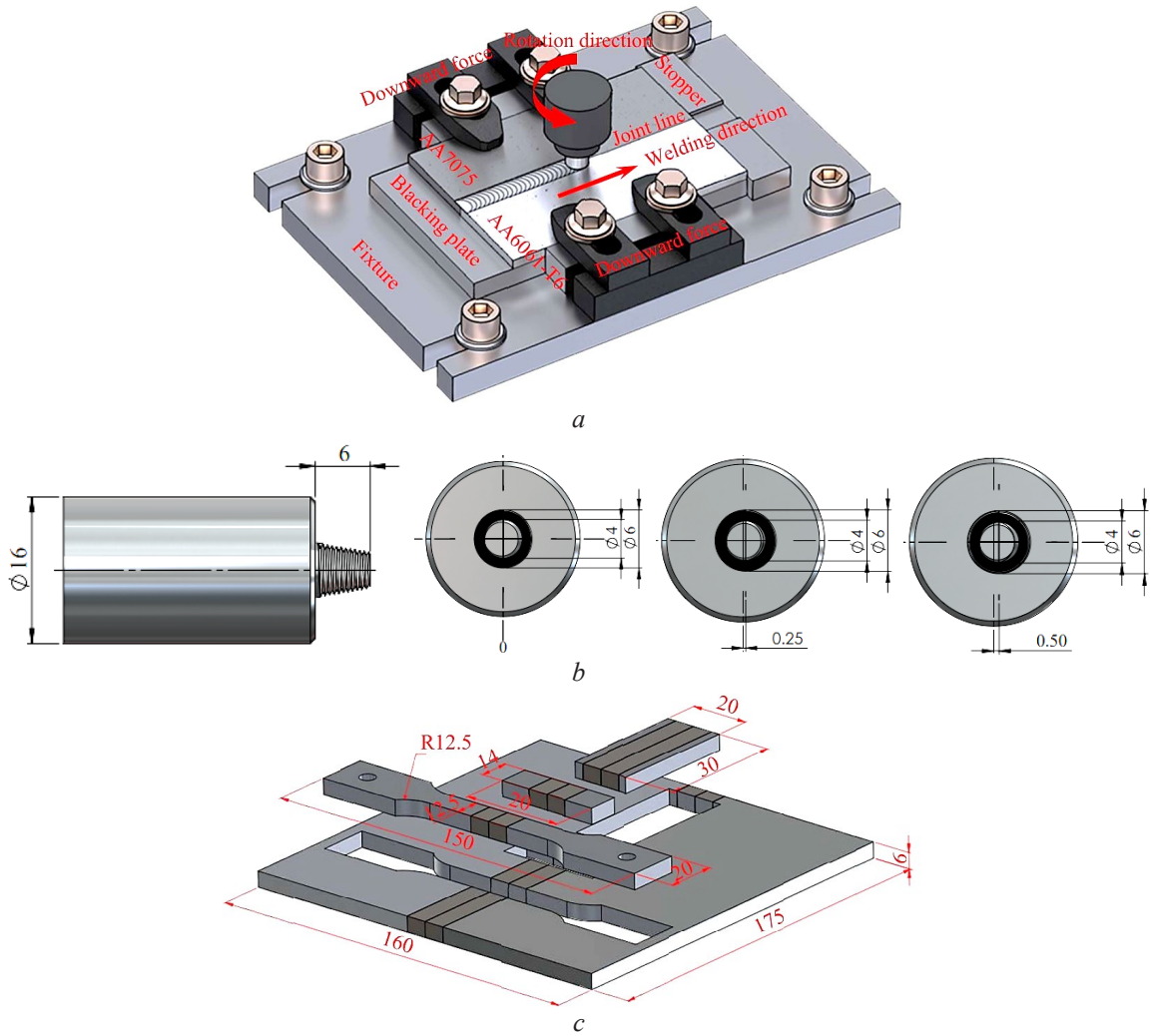

Fig. 2. Demonstrate the process in the experiment: *a* – methods of joining process; *b* – tool profile; *c* – mechanical and chemical properties testing

Table 3

Factors and parameters of the experimental

Experimental factors	Experimental level		
	–1	**0**	**1**
Rotation Speeds: *S* (rpm)	1200	1400	1600
Travel speeds: *f* (mm/min)	20	30	40
Pin eccentricity: *Te* (mm)	0	0.25	0.50

To investigate the macrostructure and microstructure, the specimens are cast in resin and then polished with emery paper in sequence, starting from P220 and progressing up to P1200. The specimen was polished with alumina powder (1–3 μm). The samples were etched with a mixture of 100 mL H_2O and 3 mL HF for 25 s. Finally, they were rinsed with distilled water and wiped clean with alcohol. A hot air gun was used to blow over the samples to dry them faster – an investigation of the macrostructure to verify weld integrity. As well as examine the microstructures of HAZ, TMAZ, and SZ with an optical microscope (OM). Finally, the joints' chemical composition and

fracture characteristics were examined by scanning electron microscopy (SEM) model TESCAN MIRA at Khon Kaen University, Thailand, using EDX mapping and point analysis techniques. Crystallite size analysis of the joint was performed using the XRD technique. The diffraction analysis machine was an X-Ray Diffractometer Model XRD 6100 2kw Shimadzu using 60 kV and 80 mA electromotive force radiation (emf). The nickel target was used. Diffraction angles greater than 120 degrees were tested for peak angle by scanning at an 80 degree angle. The specimen was prepared as a thin plate, 10×10 mm. in size. The sample is then mounted onto the XRD instrument by holding the sample firmly and in a position where the X-ray beam passes at a uniform angle.

2. 3. Experimental design

Taguchi method was used for this experimental design because the Taguchi method is a tool that can improve the product and process quality and can help to reduce time and cost effectively [33]. Taguchi's experimental design with orthogonal array L9 consisting of 3 parameters in 3 levels: rotation Speeds, travel speeds, and pin eccentricity, are shown in **Table 3.** Thereafter, the signal-to-noise (*S*/*N*) ratio was analyzed for each level of the process parameter. The *S*/*N* analysis shows a higher *S*/*N* ratio indicates better weld quality characteristics [33, 34]. Therefore, the optimal process parameter level is the one with the highest *S*/*N* ratio, with larger values being better (analysis: larger-the-better). The equations used to calculate the *S*/*N* ratio are shown in (1):

$$S/N_s = -10\log\left(\frac{1}{n}\sum_{i=1}^{n}\frac{1}{y_i^2}\right). \quad (1)$$

3. Results

3. 1. S/N ratio analysis

The effects of FSW were analyzed using tensile strength (*Ts*), elongation (% El), and joint hardness (HV). The data are converted to the mean *S*/*N* ratio, as shown in **Table 4**. The analysis using the *S*/*N* ratio of *Ts* found that the optimal level was $A_2B_1C_2$, i.e., rotation speed 1200 rpm, travel speed 20 mm/min, and pin eccentricity 0.25 mm. Similarly to the elongation of the joints, the optimum level was $A_2B_1C_2$ with an elongation of 11.12 %. Finally, the *S*/*N* ratio of hardness was analyzed, and the optimal level was $A_1B_3C_3$, with an average hardness level of 136 HV.

Table 4

Experimental of orthogonal array-L9, *S*/*N* ratio of *Ts*, % El and *HV*

No.	*S* (*A*)	*f* (*B*)	*Te* (*C*)	*Ts* (MPa)	% El	HV	*S*/*N* Ratio (*Ts*)	*S*/*N* Ratio (% El)	*S*/*N* Ratio (*HV*)
1	1000	20	0	184	6.2	122	45.30	15.85	41.73
2	1000	30	0.25	162	4.1	126	44.19	12.26	42.01
3	1000	40	0.5	140	0.5	136	43.11	–6.02	42.67
4	1200	20	0.25	216	11.2	116	46.69	20.98	41.29
5	1200	30	0.5	177	8.7	128	44.96	18 .79	42.14
6	1200	40	0	143	1.8	132	42.92	5.11	42.41
7	1400	20	0.5	201	7.4	125	46.06	17.38	41.94
8	1400	30	0	177	3.5	110	44.96	10.88	40.83
9	1400	40	0.25	148	2.1	114	43.41	6.44	41.14

Fig. 3 shows the main effects of the factors on the *S*/*N* ratio of mean tensile strength, elongation, and joint hardness. **Fig. 3, *a*,** shows the main effects of the mean factor on tensile strength and elongation. It was found that the maximum *S*/*N* ratio of rotation speeds was 1200 rpm, the maximum *S*/*N* ratio of travel speeds was 20 mm/min, and the maximum *S*/*N* ratio of pin eccentricity was 0.25 mm. Therefrom, considering the effect of the main factors on the maximum hardness of SZ, it was found that the maximum *S*/*N* ratio of rotation speeds was 1000 rpm, the maximum *S*/*N* ratio of travel speeds was 40 mm/min., and the maximum *S*/*N* ratio of pin eccentricity is 0.5 mm.

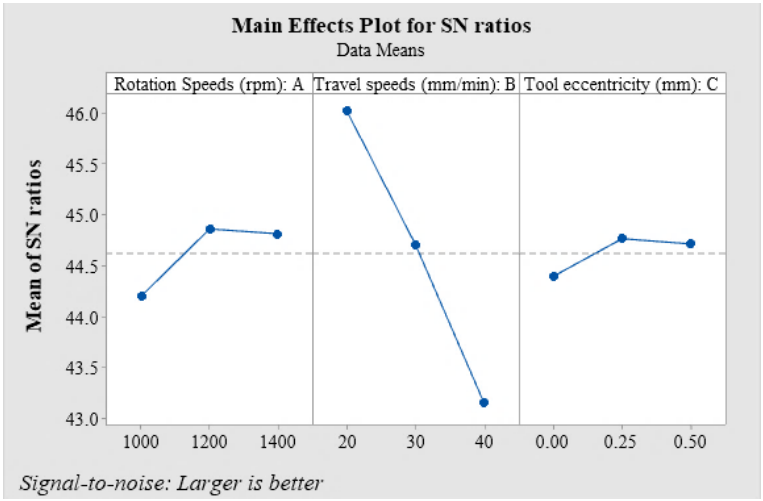

a

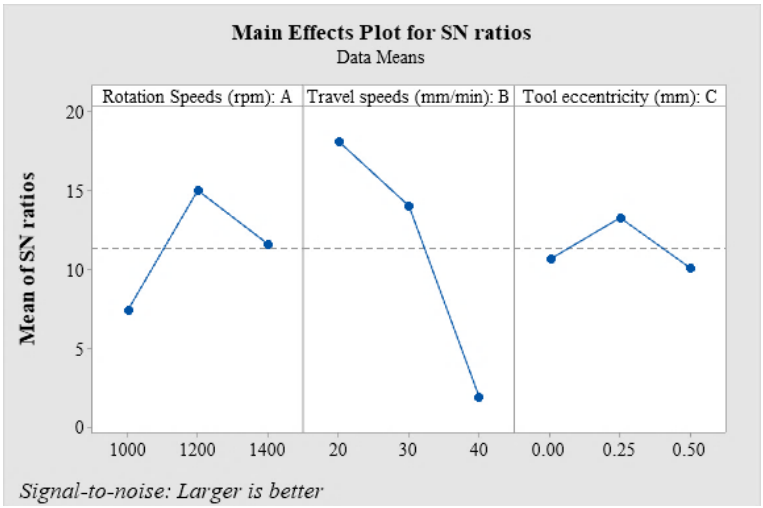

b

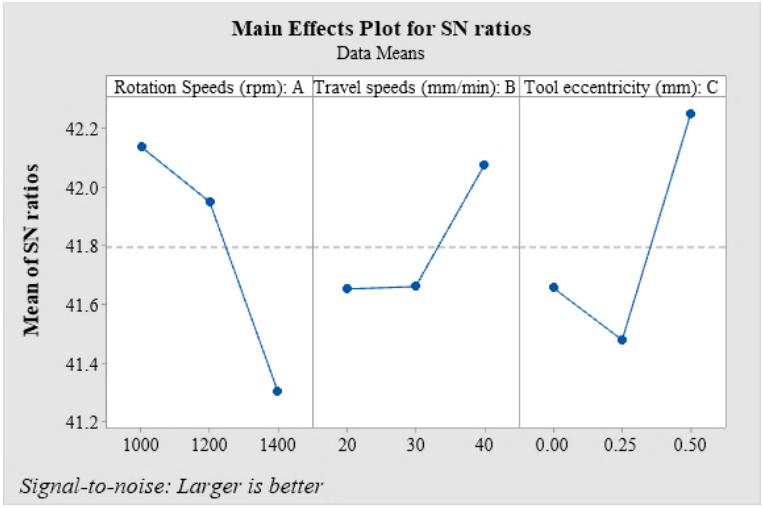

c

Fig. 3. Main effects plot for *S*/*N* ratio value: *a* – *Ts*; *b* – % El; *c* – *HV*

Thereafter, considering the *S*/*N* ratio response of the mean tensile strength, elongation, and joint hardness, as shown in **Table 5**. Analysis of the mean tensile strength and elongation found that the highest response *S*/*N* ratio of rotation speeds was 44.86 and 14.96, and the highest response

S/*N* ratio of travel speeds was 46.02 and 18.07. Finally, the pin eccentricity *S*/*N* ratio responses were the highest, 44.76 and 13.23 for the elongation rate, respectively. Thereafter, considering the *S*/*N* ratio response of joint hardness, the highest *S*/*N* ratio response of rotation speeds was 42.14, and the highest *S*/*N* ratio response of travel speeds was 42.07. Finally, the maximum pin eccentricity *S*/*N* ratio response was 42.25.

Table 5

Response Table for *S*/*N* ratios value *Ts*, % El, and *HV*

Level	Tensile strength (MPa)			% Elongation			Hardness (*HV*)		
	***S* (*A*)**	***f* (*B*)**	***Te* (*C*)**	***S* (*A*)**	***f* (*B*)**	***Te* (*C*)**	***S* (*A*)**	***f* (*B*)**	***Te* (*C*)**
1	44.20	46.02	44.39	7.36	18.07	10.61	42.14	41.65	41.66
2	44.86	44.70	44.76	14.96	13.98	13.23	41.95	41.66	41.48
3	44.81	43.14	44.71	11.57	1.84	10.05	41.30	42.07	42.25
Delta	0.66	2.87	0.37	7.60	16.23	3.18	0.83	0.42	0.77
Rank	2	1	2	2	1	2	1	3	3

3. 2. ANOVA analysis

Find the statistically significant factors using ANOVA on the process parameters on the response and the significance of the factors considered. ANOVA tables for the mean *S*/*N* ratio of tensile strength, elongation, and weld hardness are shown in **Table 6**. Analysis of variance (ANOVA) found that the factors that had the most significant effect on tensile strength and elongation were travel speed, and these three factors did not affect the mean joint hardness at a 95 % confidence level.

Table 6

Analysis of Variance for *S*/*N* ratios values *Ts*, % El, and *HV*

Source	DF	Seq SS	Adj SS	Adj MS	F	P
Tensile strength						
Rotation Speeds (rpm)	2	0.8111	0.8111	0.4055	1.86	0.350
Travel speeds (mm/min)	2	12.3992	12.3992	6.1996	28.44	0.034
Pin eccentricity (mm)	2	0.2393	0.2393	0.1196	0.55	0.646
Residual Error	2	0.4359	0.4359	0.2180	–	–
Total	8	13.8855	–	–	–	–
$S = 0.5010$, $R–Sq = 96.86$ %, $R–Sq(adj) = 87.44$ %						
% Elongation						
Rotation Speeds (rpm)	2	22.149	22.149	11.074	9.70	0.093
Travel speeds (mm/min)	2	70.002	70.002	35.001	30.67	0.032
Pin eccentricity (mm)	2	6.829	6.829	3.414	2.99	0.250
Residual Error	2	2.282	2.282	1.141	–	–
Total	8	101.262	–	–	–	–
$S = 1.0682$, $R–Sq = 97.75$ %, $R–Sq(adj) = 90.98$ %						
Hardness						
Rotation Speeds (rpm)	2	1.1485	1.1485	0.5743	2.39	0.295
Travel speeds (mm/min)	2	0.3492	0.3492	0.1746	0.73	0.579
Pin eccentricity (mm)	2	0.9834	0.9834	0.4917	2.04	0.328
Residual Error	2	0.4809	0.4809	0.2404	–	–
Total	8	2.9620	–	–	–	–
$S = 0.4903$, $R–Sq = 83.77$ %, $R–Sq(adj) = 35.06$ %						

Table 6 initially, from the analysis of variance for the *S*/*N* ratio of the mean tensile strength. It was found that the value of $R–Sq = 96.86$ %. It can be concluded that all three factors are related and affect the tensile strength of joints. Considering the *P*-value, it was found that travel speeds

had a *P*-value = 0.034, less than 0.05, in the critical zone, indicating that this factor had the most significant effect on the average tensile strength. Subordinates are rotation Speed and pin eccentricity, respectively. Subsequently, analysis of variance for the *S*/*N* ratio of mean elongation found that *R*–*Sq* = 97.75 %. It can be concluded that the three factors are related and affect joint elongation. Considering the *P*-value of travel speeds, *P*-value = 0.032 is less than 0.05 in the critical zone, indicating that this factor affects the average joint elongation. Finally, analysis of variance for the *S*/*N* ratio of the mean hardness found that *R*–*Sq* = 83.77 %, which is low. Thus, it was concluded that the three unrelated factors on the joints' hardness. Considering the P-value of the three factors, it was found that a *P*-value greater than 0.05 was not in the critical zone, indicating that it did not affect the mean joint hardness at the 95 % confidence level [33, 34].

3. 3. Predictions and experimental confirmation

The experimental parameters were obtained at the optimum levels that gave the highest tensile strength and elongation, i.e., the rotation speed of 1200 rpm and travel speed of 20 mm/min, and the pin eccentricity is 0.25 mm ($A_2B_1C_2$). On the other hand, the optimal parameters for joint hardness are rotation speed at 1000 rpm, travel speed is 40 mm/min., and pin eccentricity is 0.5 mm ($A_1B_3C_3$). The prediction of the result by regression equation is shown in (2)–(4). The response prediction by the Taguchi method and the experimental confirmation are shown in **Table 7**.

Table 7

The results of the experiments were confirmed with the statistical analysis

Response	Taguchi approach	ANOVA approach	Confirmatory experiment
Tensile strength (MPa)	209.33	200.33	208.42
Elongation (%)	11.18	16.106	10.45
Hardness (*HV*)	138.56	130.11	135.52

The results were considered for confirmation with the Taguchi method, and the regression analysis results were similar:

$$\text{Tensile strength } (Ts) = 216.7+0.0308(S)-2.833(f)+13.3(Te). \quad (2)$$

The predictive tensile strength was:

$$Ts = 216.7+0.0308(1200)-2.833(20)+13.3(0.25) = 200.33 \text{ MPa}.$$

$$\text{Elongation } (\%\ El) = 12.21+0.00183(S)-0.3400(f)+3.40(Te). \quad (3)$$

The predictive elongation was:

$$El = 12.21+0.00183(1200)-0.3400(0.25)+3.40(20) = 16.106.$$

$$\text{Hardness } (HV) = 144.6-0.0292(S)-0.317(f)+16.7(Te). \quad (4)$$

The predictive hardness was:

$$HV = 144.6-0.0292(1000)-0.317(40)+16.7(0.5) = 130.11\ HV.$$

3. 4. Tensile strength and elongation analyzer

The efficiency of the FSW process by the Taguchi method was studied. In the fourth experiment, $A_2B_1C_2$ (rotation speed is 1200 rpm, travel speed is 20 mm/min, and pin eccentricity is 0.25 mm) had the highest tensile strength. The lowest tensile strength experiment was the third

experiment, $A_1B_3C_3$ (rotation speed 1000 rpm, travel speed 40 mm/min, and pin eccentricity 0.5 mm). **Fig. 4** shows the fracture zone of the tensile specimens. In **Fig. 4, *a*,** the fracture zone of the specimen with maximum tensile strength is $A_2B_1C_2$. It was found that the fracture location occurred at the HAZ zone of the RS-AA6061 side because the HAZ region had the lowest mechanical properties compared to other regions, and fracture occurred more often at HAZ [26]. In addition, the appearance of transverse fractures was observed; shear bands at an angle of 45° to the tensile direction indicated ductile fracture characteristics resulting in high elongation. On the other hand, **Fig. 4, *b*** shows the fracture characteristics of the test specimen with the lowest tensile strength, $A_1B_3C_3$. It was found that the fracture position in the middle of the joint lowed, that the joint had lower tensile strength than the other areas. Furthermore, considering the appearance of transverse fractures, it was found that the fracture direction was perpendicular to the tensile direction, indicating that brittle damage resulted in a low elongation.

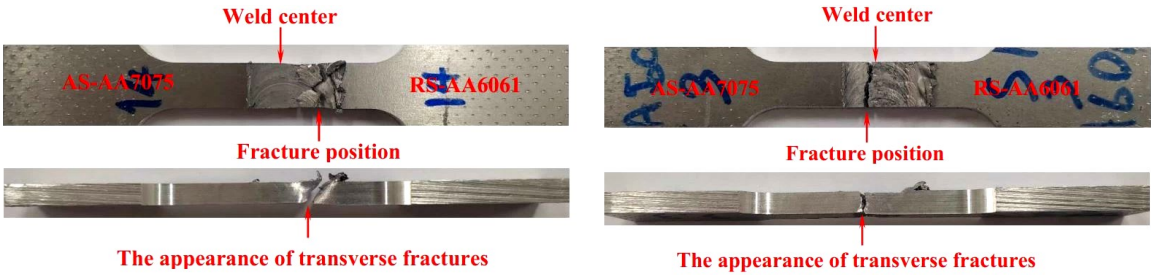

Fig. 4. Compare the fracture characteristics of the specimen *a* – $A_2B_1C_2$; *b* – $A_1B_3C_3$

3. 5. Joint hardness analysis

Fig. 5 shows the transverse hardness of the test piece at the highest joint hardness is $A_1B_3C_3$ (rotation speed 1000 rpm, travel speed 40 mm/min, and pin eccentricity 0.5 mm). The average joint hardness was 136 HV. Observe that the hardness of AA7075 is 160 HV, and AA6061-T6 is approximately 109 HV. The hardness profile of the joint was lower than the base metal on the AS side but slightly higher than the RS side. Because the SZ zone has a low hardness of AA6061 aluminum alloy, the hardness of the TMAZ and HAZ regions is not significantly different.

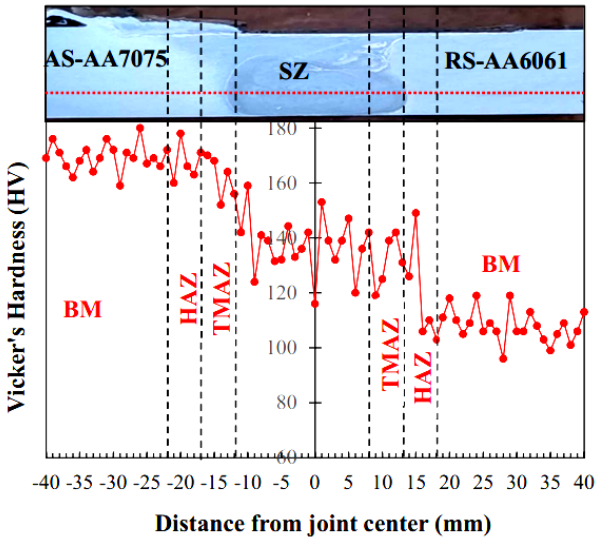

Fig. 5. Joint hardness profiles of experiments at $A_1B_3C_3$

3. 6. The macrostructure of the joints

The macrostructure of the joints in this experiment is generally an onion-ring structure. **Fig. 6** examines the macrostructure of the specimen for maximum tensile strength and minimum

tensile strength. **Fig. 6, *a*** is the $A_2B_1C_2$ specimen (rotation speed 1200 rpm, travel speed 20 mm/min, and pin eccentricity 0.25 mm). A flash defect was found on the AS side, and transversal investigations of the joint did not find defects. **Fig. 6, *b*** shows the specimen is the $A_1B_3C_3$ (rotation speed 1000 rpm, travel speed 40 mm/min, and pin eccentricity 0.5 mm). Flash defects are present on both sides, but the flash defect is higher on the RS side, and a void defect is found on the joint cross-section on the RS side. The cause is the low rotation speed and the high travel speed resulting in insufficient heat and material flow. As a result, the tensile strength of the joint decreases.

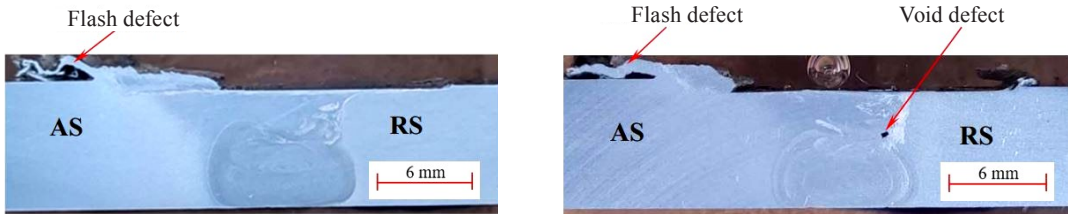

a *b*

Fig. 6. Macrostructure of specimens:
a – $A_2B_1C_2$ (maximum tensile strength); *b* – $A_1B_3C_3$ (minimum tensile strength)

3. 7. The microstructure of the joint

The joint morphology was examined by SEM technique at the experimental condition at $A_2B_1C_2$, which was the optimal parameter for this experiment. An investigation is shown in **Fig. 7** with the EDX-Mapping technique. It was found that the substrate consisted of Al, with Mg, Cu, O, and Ti as interleaved solid solution on the aluminum matrix, which is consistent with the results of the chemical composition of the base material.

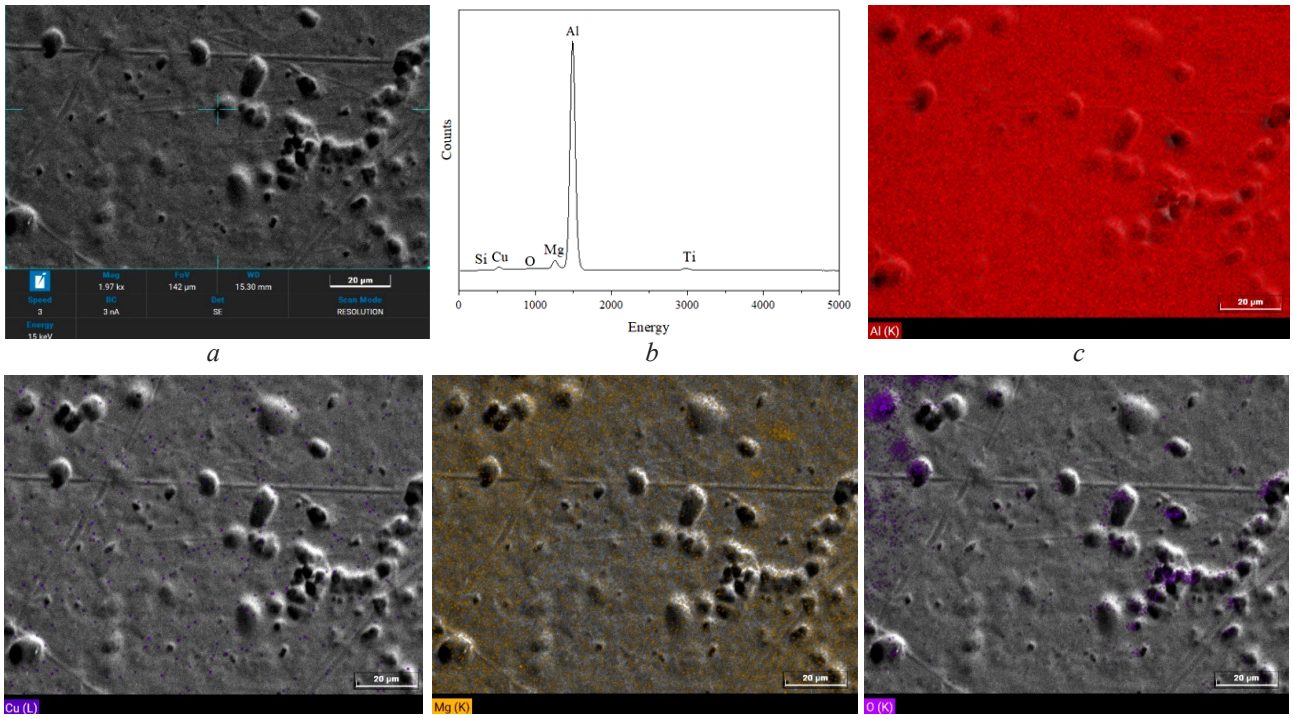

a *b* *c*

d *e* *f*

Fig. 7. Investigation of joints using EDX analysis: *a* – SEM micrographs of a joint;
b – dispersion of elements; *c* – Al; *d* – Cu; *e* – Mg; *f* – O

Fig. 8 shows an examination using the EDX-point analysis technique. An investigation of the particles formed in the welding line is shown in **Fig. 8, *b–f***. It was found that Al and Mg were

composed of Al_3Mg_2, which appeared as spherical gray on the welding surface, and the Al_2O_3 particle, which was black and non-spherical and inserted on the aluminum matrix. It is assumed that it may be caused by welding without oxygen shielding, thus forming Al_2O_3 compounds. The investigation revealed that the Al_2O_3 compound did not significantly on the mechanical properties of the coupling for this experiment. However, the volume and distribution are different when considering the particles formed in each region; for example, in **Fig. 8, *b***. It was observed that fine spherical Al_3Mg_2 particles are uniformly distributed on the joint surface. Finally, considering **Fig. 8, *c–f***, the pin-tip zone shows a decreased, non-uniform particle distribution and larger particle size.

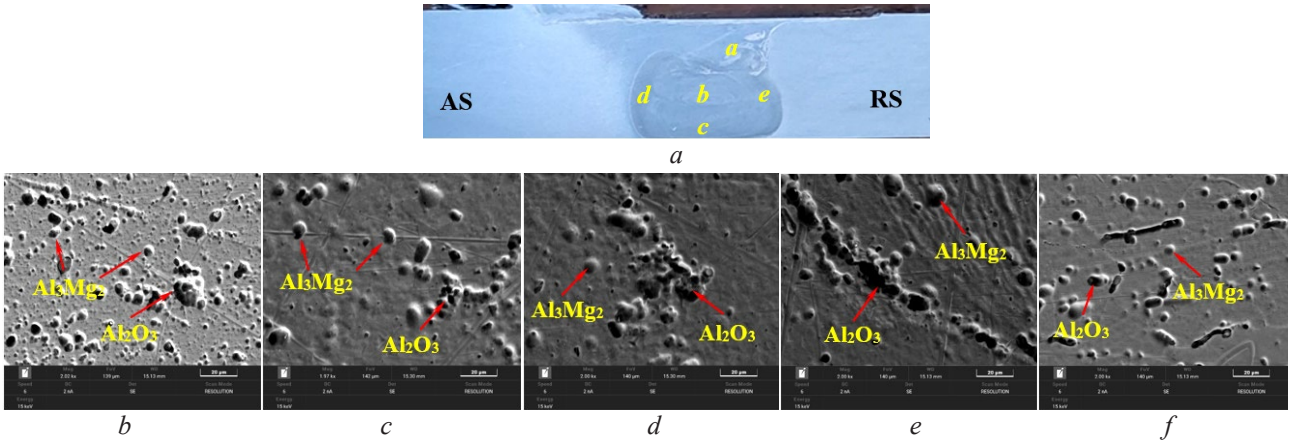

a

b *c* *d* *e* *f*

Fig. 8. The morphology of the joint by the FSW process: *a* – the position in the examine; *b* – the top zone(point *a*); *c* – center zone(point *b*); *d* – bottom zone(point *c*); *e* – TMAZ-AS side (point *d*); *f* – TMAZ-RS side (point *e*)

3. 8. Crystallite size analysis

Fig. 9 shows XRD patterns of aluminum alloys AA6061-T6 and AA7075 and $A_1B_3C_3$ and $A_2B_1C_2$ joints. Comparison with aluminum as the base material revealed that the peak of the (200) crystalline plane was observed. Thereafter, when stirred, the peak at the joint changes from the (200) plane to the (111) crystal plane in FSW due to the plastic deformation of the metal, the reorientation of the crystal lattice structure, and the formation of recrystallized grains. Finally, the peak was measured to determine the FWHM for estimating the crystal strain before establishing the slope and then calculating the crystallite size.

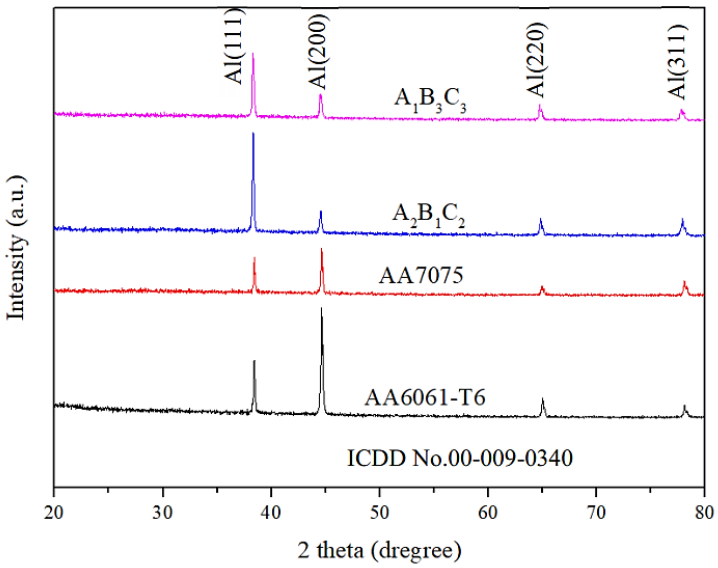

Fig. 9. The XRD patterns of the joining and base material

Fig. 10 shows the crystallite sizes of $A_1B_3C_3$ and $A_2B_1C_2$ joints with AA6061 and AA7075 aluminum alloy as base materials. The investigation found that the welding parameters affected the crystallite size of the joint. For example, in the welding condition at $A_1B_3C_3$, the crystallite size of the joint is 0.43 µm. Therefore, increasing the welding factor to the welding condition, $A_2B_1C_2$ found that the crystallite size was increased to 0.74 µm. The average crystallite size was 0.99 and 1.34 µm lower than that of the base material for AA6061 and AA7075 alloy, respectively.

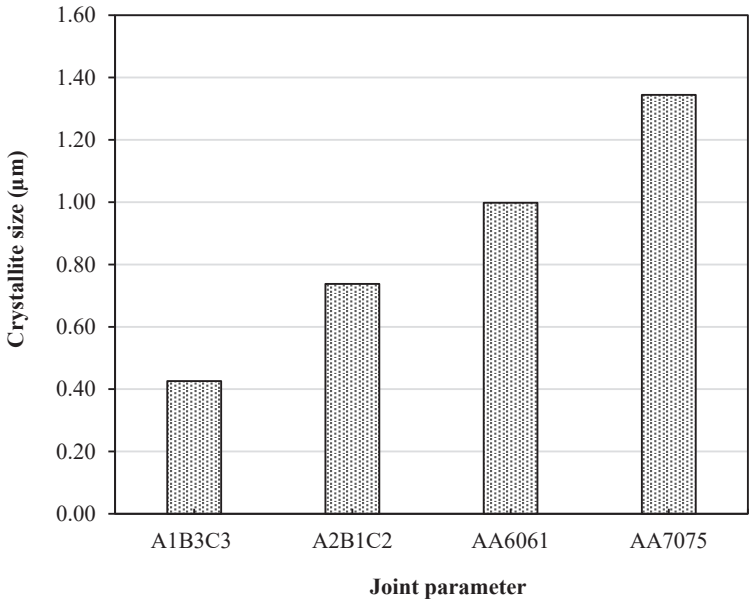

Fig. 10. The crystallite size of the joining and base material (µm)

3. 9. Fracture analysis

The tensile specimen is examined for the fracture mechanism. As shown in **Fig. 4**, the welding conditions $A_2B_1C_2$ and $A_1B_3C_3$. The fracture characteristics were found to be different, as shown in **Fig. 11**. Examine the center of the specimen for fracture on both retreating (RS) and advancing (AS) sides. **Fig. 11, *a, b*** shows the fracture characteristics of the welded tensile specimen under condition $A_2B_1C_2$ as the parameter with an ultimate tensile strength of 216 MPa. It was found that both the retreating and advancing fractures had similar fracture characteristics, with deeper and larger dimple fractures indicating ductile damage. Corresponding to **Fig. 4, *a*** the shear fracture is angled 45° to the tensile direction, suggesting the ductile fracture characteristics resulting in high elongation. On the other hand, the joint condition at $A_1B_3C_3$, the lowest tensile strength parameter, is 140 MPa. Small and fine dimple fractures are combined with cleavage fractures, both retreating and advancing brittle behavior. Consistent with **Fig. 4, *b***. the fracture line is perpendicular to the tensile direction, suggesting brittle fracture characteristics resulting in low elongation.

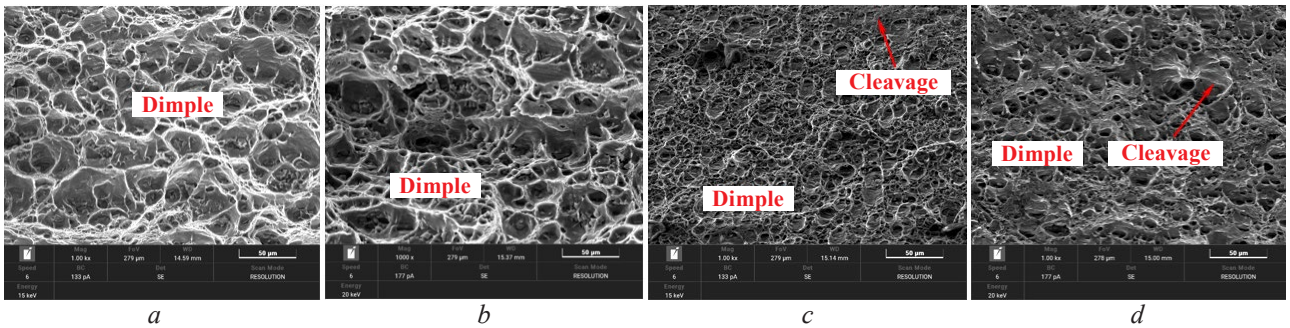

a *b* *c* *d*

Fig. 11. The fracture analyzing of the joint:
a – AS-$A_2B_1C_2$; *b* – RS-$A_2B_1C_2$; *c* – AS-$A_1B_3C_3$; *d* – RS-$A_1B_3C_3$

4. Discussion

In this study, the FSW process investigated the optimization of the dissimilar joint between AA6061-T6 and AA7075 aluminum alloy-experimental design using the Taguchi method. The experimental parameters were rotational speed (1000–1400 rpm), travel speeds (20–40 mm/min), and pin eccentricity (0–0.5 mm). The total number of experiments is 9 runs, and the response to be investigated are tensile strength, elongation, and joint hardness. According to the fabricate factor investigation, travel speeds significantly on tensile strength and elongation, but the rotational speed and pin eccentricity do not affect the tensile strength and joint elongation. Furthermore, considering the fabricated parameters on the hardness of the joint, it was found that all factors did not affect the joint hardness. Therefore, the correlation of the factors to the factor response values was analyzed using regression models at a confidence level of 0.05 ($\alpha = 0.05$). It was found that the tensile strength model had $R^2 = 96.86$, and 97.78 for elongation, respectively. However, the hardness of the joint was $R^2 = 83.77$ which is a low value, and it was concluded that the fabricate parameters did not affect the joint hardness. Therefore, analyze the optimum factor with the signal-to-noise ratio. It was found that the optimal experimental level for tensile strength and elongation was a rotational speed of 1200 rpm, travel speeds of 20 mm/min, and pin eccentricity of 0.25 mm, with mean *S*/*N* ratios of 216 MPa and 11.12 %, respectively. Then, the experiment was repeated to confirm the experimental results for five samples using the optimum factors from the *S*/*N* ratio analysis. It was found that the value obtained from the confirmation was approximate to the value obtained by the Taguchi method and the regression equation prediction.

Consider the joint's macrostructure, microstructure, chemical composition, crystallite size, and fracture characteristics. It was found that the macrostructure of the joint fabricated in condition $A_2B_1C_2$ showed no defects on the joint surface, but the weld condition at $A_1B_3C_3$ showed defects in the joint surface at the top of the joint on the TMAZ side of the RS. The defect will be the crack initiation of rapid fracture, causing the tensile strength of the joint to decrease. When considering the microstructure of the joint was using the SEM technique. It was found that in **Fig. 7, *a***, the top of the weld zone pressed by the shoulder of the tool has uniformly dispersed fine spherical particles. This may be due to the pressure on the tool shoulder and the high heat resulting in smaller, finer particles and more uniform distribution than other joint areas. Next, examine the chemical composition of the joints, containing Al, Mg, Cu, O, and Ti as the main components. For example, in investigations, Mg_2Al_3 and Al_2O_3 compounds were found in the joints, as shown in **Fig. 8**. Furthermore, crystallite size analysis found that the welding factors on the crystallite size, as shown in **Fig. 10**. And the peak at the joint changes from the (200) plane to the (111) crystal plane due to the plastic deformation of the metal and the reorientation of the crystal lattice structure during the welding process. The (200) plane is the dominant crystal plane in the base metal, and it is oriented perpendicular to the surface of the material. As the rotating tool moves along the joint line, it generates heat and applies pressure to the metal, causing plastic deformation of the material. This plastic deformation causes the (200) plane to rotate and reorient, resulting in a change in the orientation of the crystal lattice structure. During the welding process, the (200) plane undergoes a reorientation process, and the (111) crystal plane becomes the dominant crystal plane at the joint. This is because the (111) plane has a lower energy state and is more sTable than the (200) plane. As the metal deforms and the crystal lattice structure reorients, the (111) plane becomes more dominant and eventually becomes the primary crystal plane at the joint. In addition to the reorientation of the crystal lattice structure, the formation of recrystallized grains also plays a role in the change of the dominant crystal plane at the joint. Recrystallization occurs when the deformed grains are replaced by new grains that have a different orientation. This process can also contribute to the change in the dominant crystal plane at the joint.

This investigation concluded that welding parameters, such as travel speed, significantly affected the mechanical properties. Examining the joint's fracture surface revealed different surface characteristics where fracture surfaces of $A_2B_1C_2$, which is the optimal parameter for tensile strength. However, both retreating and advancing fractures have similar characteristics, with deeper and larger dimple fractures suggesting ductile damage. On the other hand, the splicing parameter $A_1B_3C_3$ was the lowest tensile strength. It is characterized by a small and fine dimple fracture combined with a cleavage fracture, which is brittle on both retreating and advancing sides.

In general, ductile materials are able to undergo plastic deformation before they fracture, while brittle materials do not undergo much plastic deformation before they fracture. Ductile materials tend to exhibit dimple fracture, while brittle materials tend to exhibit cleavage fracture. And it is possible that the $A_2B_1C_2$ specimen with the highest tensile strength was made from a material that was more ductile and, therefore, able to undergo more plastic deformation before fracturing. This would result in a dimple fracture, which is characteristic of ductile materials. On the other hand, the $A_1B_3C_3$ specimens that exhibited both dimple and cleavage fractures may have been made from a material that was less ductile and more brittle, or subjected to a more severe loading condition. This would result in both types of fractures occurring in the same specimen.

In order to study the joining of AA6061-T6 and AA7075 aluminum alloy by FSW technique for this study. To study the joining of AA6061-T6 and AA7075 aluminum alloy by FSW technique for this study. Some limitations may apply, for example: 1. The joint strength of FSWed AA6061-T6 and AA7075 aluminum alloys may not be as high as other welding methods such as GTAW or GMAW due to the lower melting point of aluminum alloys. 2. FSW is not suiTable for welding thick sections of aluminum alloys, as the heat generated during the welding process may cause distortion or other defects in the joint. 3. FSW may have limitations in terms of the joint geometry that can be produced, as the tool. geometry and welding parameters may be limited by the material thickness and shape of the workpiece. And these are the disadvantages of FSW welding process. Future study guidelines for joining dissimilar aluminum alloys between AA6061-T6 and AA7075 should be studied the optimizing tool design, process parameters, surface preparation, interlayer materials, and post-weld heat treatment. These efforts aim to improve the quality and reliability of the welds for various applications in different industries.

Finally, to demonstrate the difference between the research and other techniques. Therefore, the researcher compared the techniques as shown in **Table 8**.

Table 8
Summary of experimental data and literature reports

Ref.	Method	Material	Ts (MPa)	% El	HV	Chemical composition/ Fracture analysis	XRD analysis
[11]	N/A	AA6061/AA5083	191.62	7.32	82.8	N/A	N/A
[12]	N/A	AA2024/AA6061	N/A	N/A	N/A	Examine	Examine
[13]	Taguchi	AA5454/AA7075	218.88	N/A	N/A	N/A	N/A
[14]	N/A	AA6061-T6/AA7075-T6	212	N/A	136	Examine	N/A
[15]	N/A	AA5052/AA5J32	N/A	N/A	90	Examine	N/A
[16]	N/A	AA6082/AA2024	250	11.7	N/A	Examine	N/A
[17]	Taguchi	AA2219/AA5083	298	N/A	95	N/A	N/A
[19]	Taguchi	AA2024-T6/AA6351-T6	254	N/A	N/A	N/A	N/A
[20]	RSM	AA6061/AA5083	135	4.35	N/A	N/A	N/A
[21]	RSM	Al6061-T6 and HSS590	2.34 KN	14.04	111.10	Examine	N/A
[22]	ANOVA	AA2014/AA6063	93.72	4.36	108.3	Examine	N/A
[23]	N/A	AA6351/AA5083	N/A	N/A	N/A	N/A	N/A
[24]	N/A	SSM/AA6063	120.7	N/A	N/A	Examine	N/A
[25]	ANOVA	AA 6061-T4	160.5	8.7	N/A	Examine	N/A
[26]	ANN model	AA7075/AA5083	267	N/A	N/A	Examine	N/A
[27]	ANN model	AA5083-O–AA6063-T6	168	N/A	87	N/A	N/A
[28]	ANN model	Adaptive network-based	N/A	N/A	N/A	Examine	Examine
[29]	ANFIS–SA	AA7075	227	N/A	238	Examine	N/A
[30]	Taguchi	AA5383/AA7075	143.42	N/A	94.05	N/A	N/A
[31]	Taguchi	AA6061/AA7075	168.34	N/A	37	N/A	N/A
[32]	Taguchi	AA6061	192.58	12.59	114.5	N/A	N/A
[33]	Taguchi	AA5052/Ti-4V-6Al	2.84 KN	N/A	N/A	N/A	N/A
[34]	ANOVA	SSM 5083	235.22	N/A	80.64	Examine	N/A
This work	Taguchi	AA7075/AA6061-T6	216	29.3	135.52	Examine	Examine

It was found that most of the research focuses only on studying the mechanical properties of joints. Therefore, the chemical composition, fracture characteristics, and crystal size have not been examined.

Therefore, this study was investigated to provide observation for application and fundamental for the further study of the FSW process, and the FSW process has been found to be an effective method for joining aluminum alloys AA6061-T6 and AA7075 in industrial applications, offering advantages such as reduced distortion, improved mechanical properties, better corrosion resistance, and reduced processing time and cost.

5. Conclusions

The experimental factors showed that travel speeds significantly affected tensile and elongation, but the rotational speed and tool eccentricity did not affect tensile and elongation. Furthermore, considering the fabricate parameters on hardness, it was found that it did not affect the hardness of the joint.

The factor response relationship was analyzed using a regression model at a confidence level of 0.05. It was found that the tensile strength model had $R^2 = 96.86$, and 97.78 for elongation, respectively. On the other hand, the hardness has $R^2 = 83.77$, which is low, so it can be concluded that the manufacturing parameters do not affect the hardness of the joint.

The optimum factor with the Signal to noise ratio found that the optimum experimental conditions for tensile strength and elongation were rotational speed 1200 rpm, travel speeds 20 mm/min, and pin eccentricity 0.25 mm. The mean values were 216 MPa and 11.12 %, but the fabricate factor did not significantly affect the joint hardness.

The fracture surface of $A_2B_1C_2$, the highest tensile strength parameter, exhibits a depth dimple fracture and large size, suggesting that ductile damage occurs. On the other hand, the joint condition where $A_1B_3C_3$ is the lowest tensile parameter showed small and fine dimple fractures in conjunction with cleavage fractures.

Conflict of interest

The authors declare that they have no conflict of interest in relation to this research, whether financial, personal, authorship, or otherwise, that could affect the research and its results presented in this paper.

Financing

The study was performed without financial support.

Data availability

Data will be made available on reasonable request.

Acknowledgments

Thank you to the Division of Industrial Technology, Faculty of Industrial Technology at Nakhon Phanom University. Supporting equipment for research to be completed successfully. Moreover, we would like to thank Assistant Professor Dr. Somchat Sonasang for validating the article.

References

[1] Sarila, V., Koneru, H. P., Cheepu, M., Chigilipalli, B. K., Kantumuchu, V. C., Shanmugam, M. (2022). Microstructural and Mechanical Properties of AZ31B to AA6061 Dissimilar Joints Fabricated by Refill Friction Stir Spot Welding. Journal of Manufacturing and Materials Processing, 6 (5), 95. doi: https://doi.org/10.3390/jmmp6050095

[2] Matsuda, T., Ogaki, T., Hayashi, K., Iwamoto, C., Nozawa, T., Ohata, M., Hirose, A. (2022). Fracture dominant in friction stir spot welded joint between 6061 aluminum alloy and galvannealed steel based on microscale tensile testing. Materials & Design, 213, 110344. doi: https://doi.org/10.1016/j.matdes.2021.110344

[3] Karthikeyan, R. (2021). Establishing relationship between optimised friction stir spot welding process parameters and strength of aluminium alloys. Advances in Materials and Processing Technologies, 8 (1), 1173–1195. doi: https://doi.org/10.1080/2374068x.2020.1855401

[4] Zhang, G., Xiao, C., Ojo, O. O. (2021). Dissimilar friction stir spot welding of AA2024-T3/AA7075-T6 aluminum alloys under different welding parameters and media. Defence Technology, 17 (2), 531–544. doi: https://doi.org/10.1016/j.dt.2020.03.008

[5] Reimann, M., Goebel, J., dos Santos, J. F. (2017). Microstructure and mechanical properties of keyhole repair welds in AA 7075-T651 using refill friction stir spot welding. Materials & Design, 132, 283–294. doi: https://doi.org/10.1016/j.matdes.2017.07.013

[6] Mercan, E., Ayan, Y., Kahraman, N. (2020). Investigation on joint properties of AA5754 and AA6013 dissimilar aluminum alloys welded using automatic GMAW. Engineering Science and Technology, an International Journal, 23 (4), 723–731. doi: https://doi.org/10.1016/j.jestch.2019.11.004

[7] Arghode, V. K., Kumar, A., Sundarraj, S., Dutta, P. (2008). Computational Modeling of GMAW Process for Joining Dissimilar Aluminum Alloys. Numerical Heat Transfer, Part A: Applications, 53 (4), 432–455. doi: https://doi.org/10.1080/10407780701632585

[8] Çam, G., Javaheri, V., Heidarzadeh, A. (2022). Advances in FSW and FSSW of dissimilar Al-alloy plates. Journal of Adhesion Science and Technology, 37 (2), 162–194. doi: https://doi.org/10.1080/01694243.2022.2028073

[9] Abd Elnabi, M. M., El Mokadem, A., Osman, T. (2022). Optimization of process parameters for friction stir welding of dissimilar aluminum alloys using different Taguchi arrays. The International Journal of Advanced Manufacturing Technology, 121 (5-6), 3935–3964. doi: https://doi.org/10.1007/s00170-022-09531-3

[10] Texier, D., Atmani, F., Bocher, P., Nadeau, F., Chen, J., Zedan, Y. et al. (2018). Fatigue performances of FSW and GMAW aluminum alloys welded joints: Competition between microstructural and structural-contact-fretting crack initiation. International Journal of Fatigue, 116, 220–233. doi: https://doi.org/10.1016/j.ijfatigue.2018.06.020

[11] Kumar, P. S., Chander, M. S. (2021). Effect of tool pin geometry on FSW dissimilar aluminum alloys – (AA5083 & AA6061). Materials Today: Proceedings, 39, 472–477. doi: https://doi.org/10.1016/j.matpr.2020.08.204

[12] Moradi, M. M., Jamshidi Aval, H., Jamaati, R., Amirkhanlou, S., Ji, S. (2018). Microstructure and texture evolution of friction stir welded dissimilar aluminum alloys: AA2024 and AA6061. Journal of Manufacturing Processes, 32, 1–10. doi: https://doi.org/10.1016/j.jmapro.2018.01.016

[13] Abd Elnabi, M. M., Elshalakany, A. B., Abdel-Mottaleb, M. M., Osman, T. A., El Mokadem, A. (2019). Influence of friction stir welding parameters on metallurgical and mechanical properties of dissimilar AA5454–AA7075 aluminum alloys. Journal of Materials Research and Technology, 8 (2), 1684–1693. doi: https://doi.org/10.1016/j.jmrt.2018.10.015

[14] Saravanan, V., Rajakumar, S., Muruganandam, A. (2016). Effect of Friction Stir Welding Process Parameters on Microstructure and Mechanical Properties of Dissimilar AA6061-T6 and AA7075-T6 Aluminum Alloy Joints. Metallography, Microstructure, and Analysis, 5 (6), 476–485. doi: https://doi.org/10.1007/s13632-016-0315-8

[15] Song, S.-W., Kim, B.-C., Yoon, T.-J., Kim, N.-K., Kim, I.-B., Kang, C.-Y. (2010). Effect of Welding Parameters on Weld Formation and Mechanical Properties in Dissimilar Al Alloy Joints by FSW. MATERIALS TRANSACTIONS, 51 (7), 1319–1325. doi: https://doi.org/10.2320/matertrans.m2010032

[16] Cavaliere, P., De Santis, A., Panella, F., Squillace, A. (2009). Effect of welding parameters on mechanical and microstructural properties of dissimilar AA6082–AA2024 joints produced by friction stir welding. Materials & Design, 30 (3), 609–616. doi: https://doi.org/10.1016/j.matdes.2008.05.044

[17] Koilraj, M., Sundareswaran, V., Vijayan, S., Koteswara Rao, S. R. (2012). Friction stir welding of dissimilar aluminum alloys AA2219 to AA5083 – Optimization of process parameters using Taguchi technique. Materials & Design, 42, 1–7. doi: https://doi.org/10.1016/j.matdes.2012.02.016

[18] Yunus, M., Alsoufi, M. S. (2015). A statistical analysis of joint strength of dissimilar aluminium alloys formed by friction stir welding using taguchi design approach, anova for the optimization of process parameters. IMPACT: International Journal of Research in Engineering & Technology (IMPACT: IJRET), 3 (7), 61–68. Available at: https://www.researchgate.net/publication/286776287_A_Statistical_Analysis_of_Joint_Strength_of_dissimilar_Aluminium_Alloys_Formed_by_Friction_Stir_Welding_using_Taguchi_Design_Approach_ANOVA_for_the_Optimization_of_Process_Parameters

[19] Murali Krishna, P., Ramanaiah, N., Prasada Rao, K. (2013). Optimization of process parameters for friction Stir welding of dissimilar Aluminum alloys (AA2024 -T6 and AA6351-T6) by using Taguchi method. International Journal of Industrial Engineering Computations, 4, 71–80. doi: https://doi.org/10.5267/j.ijiec.2012.011.002

[20] Harachai, K., Prasomthong, S. (2023). Investigation of the optimal parameters for butt joints in a friction stir welding (FSW) process with dissimilar aluminium alloys. Materials Research Express, 10 (2), 026514. doi: https://doi.org/10.1088/2053-1591/acbb54

[21] Silachai, A., Prasomthong, S. (2022). Optimized parameter of dissimilar joining between Al6061-T6 and height-strength steel with friction stir spot welding process (FSSW). Journal of Metals, Materials and Minerals, 32 (4), 118–127. doi: https://doi.org/10.55713/jmmm.v32i4.1538

[22] Ramamurthy, M., Balasubramanian, P., Senthilkumar, N., Anbuchezhiyan, G. (2022). Influence of process parameters on the microstructure and mechanical properties of friction stir welds of AA2014 and AA6063 aluminium alloys using response surface methodology. Materials Research Express, 9 (2), 026528. doi: https://doi.org/10.1088/2053-1591/ac5777

[23] Palanivel, R., Laubscher, R., Vigneshwaran, S., Dinaharan, I. (2016). Prediction and optimization of the mechanical properties of dissimilar friction stir welding of aluminum alloys using design of experiments. Proceedings of the Institution of Mechanical Engineers, Part B: Journal of Engineering Manufacture, 232 (8), 1384–1394. doi: https://doi.org/10.1177/0954405416667404

[24] Meengam, C., Sillapasa, K. (2020). Evaluation of Optimization Parameters of Semi-Solid Metal 6063 Aluminum Alloy from Friction Stir Welding Process Using Factorial Design Analysis. Journal of Manufacturing and Materials Processing, 4 (4), 123. doi: https://doi.org/10.3390/jmmp4040123

[25] Heidarzadeh, A., Khodaverdizadeh, H., Mahmoudi, A., Nazari, E. (2012). Tensile behavior of friction stir welded AA 6061-T4 aluminum alloy joints. Materials & Design, 37, 166–173. doi: https://doi.org/10.1016/j.matdes.2011.12.022

[26] Shojaeefard, M. H., Behnagh, R. A., Akbari, M., Givi, M. K. B., Farhani, F. (2013). Modelling and Pareto optimization of mechanical properties of friction stir welded AA7075/AA5083 butt joints using neural network and particle swarm algorithm. Materials & Design, 44, 190–198. doi: https://doi.org/10.1016/j.matdes.2012.07.025

[27] Gupta, S. K., Pandey, K., Kumar, R. (2016). Artificial intelligence-based modelling and multi-objective optimization of friction stir welding of dissimilar AA5083-O and AA6063-T6 aluminium alloys. Proceedings of the Institution of Mechanical Engineers, Part L: Journal of Materials: Design and Applications, 232 (4), 333–342. doi: https://doi.org/10.1177/1464420715627293

[28] Dewan, M. W., Huggett, D. J., Warren Liao, T., Wahab, M. A., Okeil, A. M. (2016). Prediction of tensile strength of friction stir weld joints with adaptive neuro-fuzzy inference system (ANFIS) and neural network. Materials & Design, 92, 288–299. doi: https://doi.org/10.1016/j.matdes.2015.12.005

[29] Babajanzade Roshan, S., Behboodi Jooibari, M., Teimouri, R., Asgharzadeh-Ahmadi, G., Falahati-Naghibi, M., Sohrabpoor, H. (2013). Optimization of friction stir welding process of AA7075 aluminum alloy to achieve desirable mechanical properties using ANFIS models and simulated annealing algorithm. The International Journal of Advanced Manufacturing Technology, 69 (5-8), 1803–1818. doi: https://doi.org/10.1007/s00170-013-5131-6

[30] Shunmugasundaram, M., Nagarajan, S. M., Reddy, Y., Chaurasiya, P. K., Kumar, A., Rajak, U. (2021). An Experimental Study and Joining Parameters Optimization of Friction Stir Weld Butt Joint by Taguchi Approach to Maximize the Mechanical Properties. Arabian Journal for Science and Engineering, 47 (7), 8601–8615. doi: https://doi.org/10.1007/s13369-021-06352-6

[31] Seshu Kumar, G. S. V., Kumar, A., Rajesh, S., Chekuri, R. B. R., Ramakotaiah, K. (2022). An experimental study and parameter optimization of FSW for welding dissimilar 6061 and 7075 Al-alloys. International Journal on Interactive Design and Manufacturing (IJIDeM), 17 (1), 215–223. doi: https://doi.org/10.1007/s12008-022-00913-1

[32] Kumar, R. R., Singh, A., Kumar, A., Ansu, A. kumar, Kumar, A., Kumar, S., Kumar, D. et al. (2022). Enhancement of friction stir welding characteristics of alloy AA6061 by design of experiment methodology. International Journal on Interactive Design and Manufacturing (IJIDeM). doi: https://doi.org/10.1007/s12008-022-01106-6

[33] Prasomthong, S., Kaewchaloon, A., Charonerat, S. (2022). Optimization of friction stir spot welding between aluminium alloys and titanium alloy by the Taguchi method. SNRU Journal of Science and Technology, 14 (3), 245169. doi: https://doi.org/10.55674/snrujst.v14i3.245169

[34] Nakowong, K., Sillapasa, K. (2021). Optimized Parameter for Butt Joint in Friction Stir Welding of Semi-Solid Aluminum Alloy 5083 Using Taguchi Technique. Journal of Manufacturing and Materials Processing, 5 (3), 88. doi: https://doi.org/10.3390/jmmp5030088

[35] Cong, N. T., Thoa, P. T. T., Tien, D. H. (2021). Research of multi-response optimization of milling process of hardened S50C steel using minimum quantity lubrication of Vietnamese peanut oil. EUREKA: Physics and Engineering, 6, 74–88. doi: https://doi.org/10.21303/2461-4262.2021.001774

[36] Thinh, H. X., Trung, D. D. (2022). A research on application of the measurement of alternatives and ranking according to compromise solution method for multi-criteria decision making in the grinding process. EUREKA: Physics and Engineering, 2, 101–110. doi: https://doi.org/10.21303/2461-4262.2022.002120

[37] Trung, D. D., Ha, L. D. (2022). Research on selection of abrasive grain size and cutting parameters when grinding of interrupted surface using aluminum oxide grinding wheel with ceramic binder. EUREKA: Physics and Engineering, 1, 93–102. doi: https://doi.org/10.21303/2461-4262.2022.002058

Received date 17.02.2023
Accepted date 23.04.2023
Published date 25.05.2023

How to cite: *Pookamnerd, Y., Thosa, P., Charonerat, S., Prasomthong, S. (2023). Development of mechanical property prediction model and optimization for dissimilar aluminum alloy joints with the friction stir welding (FSW) process. EUREKA: Physics and Engineering, 3, 112–128. doi: https://doi.org/10.21303/2461-4262.2023.002776*